RSC Advances

PAPER

View Article Online
View Journal | View Issue

Cite this: *RSC Adv.*, 2025, **15**, 35899

Interfacial engineering based on an Al_2CO and SiC heterostructure to explore the gas sensing mechanism using first-principles strategies

Abdul Majid, *[a] Nimra Zaib Raza,[a] Amina Shehbaz,[a] Irtaza Tahir,[a] Muhammad Isa Khan[b] and Najam al Hassan[c]

Two-dimensional (2D) materials and their van der Waals (vdW) heterostructures have been considered promising for application as gas detecting devices owing to their distinct physical and chemical characteristics. In this work, we theoretically investigated Al_2CO/SiC heterostructure using semiconductor SiC as a substrate by density functional theory (DFT) calculations to explore its potential for outstanding performance. Our research focused on the comparative analysis of the adsorption properties of six gas molecules (H_2, NH_3, SO_2, NO, O_2, and H_2O) with SiC and its heterostructure. The structural properties, electronic properties, charge transfer mechanism, dynamic and thermal stabilities of the heterostructure were investigated by geometry optimization, single-point calculation, Hirshfeld charge analysis, phonon spectra and *ab initio* molecular dynamics calculations, respectively. The adsorption configurations for all adsorbed gases and work functions (WFs) were calculated to explore the sensing performance of the Al_2CO/SiC heterostructure. Our findings indicated semiconductor behavior after the formation of the Al_2CO/SiC heterostructure. Interestingly, the Al_2CO/SiC heterostructure was investigated for its adsorption of gas molecules (H_2, NH_3, SO_2, NO, O_2, and H_2O) and was found to be sensitive to the chemisorption of NH_3, SO_2, NO, O_2, and H_2O with average adsorption energy (E_{ads}) and a significant amount of charge transfer. The Al_2CO/SiC gas sensor demonstrated a recovery time of 1.84×10^2 and 0.27 s for detecting NO and NH_3 respectively. Furthermore, compared to the SiC monolayer the heterostructure Al_2CO/SiC illustrates excellent potential for application as a gas sensor to detect NO and NH_3 gases.

Received 3rd August 2025
Accepted 13th September 2025

DOI: 10.1039/d5ra05654c

rsc.li/rsc-advances

1. Introduction

Nowadays, gas sensors have received significant interest owing to their utilization for detecting hazardous gases, environmental monitoring, personal health care, food safety and indoor air quality inspection. The demand for innovative materials and gas sensors is increasing due to their reliability, high sensitivity and advanced technology. The rapid increase in industrial and human activities is caused by the discharge of hazardous gases into the environment which causes severe effects on human and animal health.[1,2] Gas detectors are crucial in different fields including air quality inspection, industry, breath analysis, agriculture and the detection of hazardous gases.[3,4] It is necessary to detect and trap dangerous gases such as NO, NO_2, SO_2, CO, and H_2S due to their increasing rates of pollution and medical applications.[5] Environmental degradation is one of the major challenges for human civilization because one-eighth of creatures die prematurely owing to acid rain, air pollution, ozone depletion and global warming.[6,7] Gas sensors are crucial for the detection and control of the quantity of dangerous gases in the air and for efficiently monitoring pollution and improving the environment. The high levels of air pollution in different regions have many different forms and complex sources that significantly hinder sustainable socioeconomic development and endanger public health. Therefore, there is a great demand for gas sensor materials which highlights the need to explore 2D gas sensors with remarkable performance owing to their huge specific surface areas, unique electrical characteristics, rapid carrier mobility, and low energy consumption.[8–10] The 2D layered materials have enormous potential for developing next-generation gas sensors but there are still challenges to be addressed, including sensitivity, accuracy, response time, selectivity, detection limit, recovery time (τ), durability, maintenance and cost.[11,12] The τ is influenced by the interactions between gas molecules and the adsorptive material and a larger τ indicates stronger adsorption which is known as chemisorption which becomes a challenge for gas desorption from surfaces. Therefore, this kind of gas

[a]*Department of Physics, University of Gujrat, Gujrat 50700, Pakistan. E-mail: abdulmajid40@yahoo.com*

[b]*Department of Physics, Rahim Yar Khan Campus, The Islamia University of Bahawalpur, Bahawalpur, Pakistan*

[c]*Department of Physics, Hazara University, Mansehra, KPK, Pakistan*

sensor cannot be discarded or reused. However, the ability to identify gas molecules is limited due to poor physisorption, which results in limited sensitivity.[13,14]

The various types of solid-state gas sensors including electrochemical,[15,16] optical,[17] electrical,[18,19] thermoelectric,[20,21] and calorimetric,[22,23] have been developed to address the obstacles of minimal concentration and rapid detection of gas molecules. The electrically transformed devices have received much attention due to their easy operation, inexpensiveness, low power consumption, portability, capacity to monitor signals in real-time and compatibility with other frequently used electronic devices.[24] In the past decade, 2D nanomaterials have gained significant attention in gas sensor applications owing to their superior properties such as higher carrier mobility, surface area, thermodynamic stability, electrical conductivity and gas adsorption ability.[25–27] The successful synthesis of single-layer graphene has enabled the research of 2D materials and previous studies have demonstrated that the graphene band gap makes it unstable for gas sensing applications but various strategies like doping, hydrogenation, construction of nanoribbons and defect engineering are being used to improve the electronic properties.[24,28,29] The remarkable mechanical and electrical properties of graphene stem from its hexagonal crystal structure, making it a potential material for a wide range of applications.[29,30] Leenaerts *et al.* utilized a first-principles methodology to study the adsorption behavior of various gases (H_2O, NH_3, CO, NO_2, and NO) on a graphene substrate.[31] Ao *et al.* discovered that CO has a weak adsorption capacity and small binding energy with graphene.[32] Prior research has shown that 2D carbon-based materials possess outstanding characteristics with incredibly thin atomic thicknesses making them suitable for various applications such as gas sensors and material adsorption. This gives them a distinct advantage in the development of new gas sensors.[33] The recently developed metal carbonyl Al_2CO has become well-known due to its distinct electronic characteristics.[34] In particular, the monolayer has been successfully synthesized and its potential for gas sensing applications is currently unknown. Metal oxides are used as the gas-detecting material in conventional sensors.[5,35] The 2D layered material exhibits unique 2D geometry a huge surface-to-volume ratio and exceptional physical and chemical properties that depend on thickness and diversity.[36,37] Similarly, 2D SiC reveals strong mechanical as well as thermal stability, large band gaps and semiconducting characteristics with a non-buckled honeycomb structure resembling graphene.[38] The SiC monolayer (ML) has attracted remarkable interest due to its exceptional chemical inertness and its fast charge transfer rate, making it possible to design a gas sensor with rapid τ and response times.[39] SiC-based technology has been widely used in gas sensors because Si–C bonds favor sp^2 hybridization, which enhances its sensing ability.[40,41] Dong *et al.* explored the gas-detecting characteristics of siligraphene for 12 different gas molecules, indicating that g-SiC_5 is a promising gas sensor for sensing HCHO, NO, and SO_2 due to its ability to be chemisorbed.[42] First-principle DFT simulations were used to investigate the chemisorption behavior of NO_2 on SiC by Gao *et al.*,[43] and Zhao *et al.* analyzed the gas-detecting properties of ML and bilayer SiC.[44] Their findings demonstrate that the SiC ML is used as an effective gas detector for NH_3 and the SiC bilayer has remarkable performance for NO_2, NO, and NH_3 gases. Wu *et al.* demonstrated the sensing mechanism of HCN and CO for SiC ML.[45] According to Babar *et al.*,[46] high sensitivity of NH_3 and CO gases can be achieved using the C_3Si ML. 2D-based functional nanodevices have great potential in various fields such as biology, chemistry, optics, mechanics, and sensing for both in concept and lab testing. They offer excellent interface quality and adjustments in electronic transport performance by modifying the material interface and controlling the structure.[47,48] The WS_2-Au-BP heterostructures demonstrated outstanding consistency and sensitivity at ambient temperature for small NO_2 concentrations. Therefore, the increasing demand for gas-sensing technology has led to the search for new functional heterostructures.[49–53]

This study presents a comprehensive theoretical analysis of the ability of the SiC ML and its heterostructure with Al_2CO to detect gases. The vdW heterostructures are designed to improve sensing performance due to their properties and potential applications in various fields which are not present in bulk and bilayer semiconductors.[54] This study has analyzed the sensing mechanism of the SiC ML and the Al_2CO/SiC heterostructure for air components and toxic gases (H_2O, NH_3, SO_2, NO, O_2, and H_2). We systematically investigated the adsorption properties of the ML and the heterostructure, and suitable adsorption sites were determined for every single molecule. The structural, electronic, phonon and *ab initio* molecular dynamics (AIMD) simulations were performed to investigate the structural properties, band structure before and after adsorption, phonon spectra, and thermal stability. For comparison and scientific discussion, the E_{ads}, adsorption distance, WF, and charge transfer integral between the surface and molecule were also calculated to investigate the sensitivity of the gas sensor. Our findings suggest that the Al_2CO/SiC heterostructure is a promising gas sensor compared to the SiC ML.

2. Computational details

The study utilized DFT to investigate the gas sensing properties of the Al_2CO/SiC heterostructure using first-principles calculations in the Amsterdam Density Functional-based BAND program.[55] The ADF-BAND program utilizes a linear combination of atomic orbitals (LCAOs) and Slater-type orbitals (STOs) to accurately analyze the structures and energy calculations. The ADF-BAND employs the numerical atomic orbitals (NAOs) technique for frozen core approximation, providing predictions in none, medium, large, and small forms.[56] The "none" option was utilized in all simulations to include all-electron interactions for determining adsorption energies. The quadratic tetrahedron technique was used to integrate the Brillouin zone and for Hamiltonian matrix elements, it employs the numerical Gaussian integration methodology. The triple zeta quality with one polarization function (TZP) was utilized for all computations to accurately analyze the electron density.[57,58] The Perdew Burke Ernzerhof (GGA-PBE) exchange–correlation functional was used for all geometry optimizations, while Grimme's DFT-

D3 technique was employed for calculations involving interlayer vdW interactions to enhance accuracy.[59]

For geometry optimizations, energy, step, and gradient convergence criterian were set to 1×10^{-6} eV, 0.01 Å, and 10^{-3} eV Å^{-1}, respectively. The electronic properties such as DOS and band structure were determined through single-point calculations after optimizing lattice parameters, bond lengths and angles using GGA PBE-D3. The phonon spectrum was calculated to confirm the dynamical stability of the heterostructure, while AIMD simulations were performed using an *NVT* canonical ensemble at 300 and 500 K to study its thermal stability.[60] The Nose–Hoover chain (NHC) thermostat was used during AIMD simulations, which regulated the temperature of the system to retain an appropriate temperature over time, while 10 000 steps with 1.0 fs (10 ps) time steps were used to equilibrate the Al_2CO/SiC heterostructure.

First, we investigated Al_2CO and SiC's pristine ML. The hexagonal lattice structure of Al_2CO consists of two Al atoms each associated with two C and O atoms. On the other hand, the SiC ML provides a planner honeycomb structure with alternating Si and C atoms, which has been suggested as stable. The gas-sensing properties were first investigated by adsorbing gas molecules (H_2O, NH_3, SO_2, NO, O_2, and H_2) on the pristine SiC ML. After determining numerous potential sites, we selected the energetically favorable site that provides the least E_{ads}. Next, four different stacking configurations of the heterostructure were analyzed to study the structural stability and choose the most stable stacking sequence with Al above the Si atom. To prevent interactions among periodic images, a vacuum distance of 20 Å was introduced. The Al_2CO/SiC heterostructure, consisting of 3×3 supercells, was optimized which yielded a low lattice mismatch of 4% and 1.8 Å interlayer separation. The lattice mismatch of the heterostructure was calculated using the formula shown in eqn (1).[61]

$$\text{Lattice mismatch}\% = \frac{a_{Al_2CO} - a_{SiC}}{a_{Al_2CO}} \times 100 \quad (1)$$

where a_{Al_2CO} and a_{SiC} represent the lattice parameters of pristine Al_2CO and SiC MLs. After the successful formation of the heterostructure, the E_{ads} for all adsorbed molecules were calculated using the following formula.[62]

$$E_{ads} = E_{Al_2CO/SiC} + E_{gas} - E_{Al_2CO/SiC+gas} \quad (2)$$

The energies of overall gas molecules adsorbed on the Al_2CO/SiC heterostructure, isolated heterostructure and gas molecules are represented by $E_{Al_2CO/SiC+gas}$, $E_{Al_2CO/SiC}$, and E_{gas} respectively. The usage of the formula in the form of $E_{ads} = E_{reactants} - E_{products}$ indicates that positive E_{ads} values address favorable and exothermic reactions. It will bring comparative clarity in the calculated values, where a larger positive number points to a more favorable reaction.

This study analyzes the gas-detecting properties and compares them with the heterostructure as a gas sensor, indicating improved properties. The Hirshfeld charge analysis was utilized to determine the charge transfer mechanism between adsorbed gas molecules and surfaces, highlighting the significant influence of their interaction mechanism. As a result, we determined how many electrons were transported from the surface to the gas molecules. The structural properties, E_{ads}, and charge transfer mechanism were used to determine the sensitivity and selectivity of the Al_2CO/SiC heterostructure for various adsorbed gases. The sensitivity (S) for the gas sensing application was calculated by using the following formula:

$$S = \frac{|WF_{absorbed} - WF_{pristine}|}{WF_{pristine}} \times 100\% \quad (3)$$

where $WF_{pristine}$ is the work function of the Al_2CO/SiC heterostructure before adsorption and its reported value is 3.89 eV. $WF_{absorbed}$ is the work function after adsorption. The detailed computational details related to the heterostructures used in this work can be found elsewhere.[63]

3. Results and discussion

The primary objectives of this study were to assess the Al_2CO side of the Al_2CO/SiC heterostructure because initial calculations on the pure SiC monolayer showed limited gas adsorption which reduced its sensing effectiveness. Although adsorption on the pure Al_2CO monolayer can potentially yield insightful information, the current study highlights how the heterostructure strengthens interactions more than the individual layers can. The detailed analysis is described in the following.

3.1 Structural and electronic properties

To investigate the potential of Al_2CO/SiC heterostructures as gas-detecting materials, we observed properties of individual MLs. The structural properties are described elsewhere in agreement with the previous studies.[63] The heterostructure of Al_2CO/SiC was created through the systematic arrangement of single Al_2CO and SiC MLs. The electronic properties of these MLs were examined using calculated band structure and DOS analysis revealing 2.5 eV direct band gap for SiC consistent with previous findings.[44] The detailed structural and electronic properties of the component monolayers and the heterostructure have been published elsewhere.[63] The DOS analysis revealed that the valence band (VB) is dominated by C atoms in 2p states while the conduction band (CB) is dominated by Si atoms in 3p states. The band gap and DOS analysis for Al_2CO revealed that Al significantly contributes to the CB with 3p states. In contrast, C and O atoms significantly contribute to the VB with 2p states compared to the CB, and the PDOS of both ML were discussed and plotted in detail, consistent with previous findings.[63]

To investigate the structural stability of the Al_2CO/SiC heterostructure, different stacking configurations were analyzed by placing atoms in various positions. The analysis of binding energy indicates that AB stacking of the Al_2CO/SiC heterostructure is the most stable and thus used for gas sensing applications. The interlayer separation between the heterostructures is 1.80 Å, representing the strong interaction between MLs.

$$E_b = E_{Al_2CO/SiC} - E_{Al_2CO} - E_{SiC} \quad (4)$$

$$W_{ad} = (E_{Al}^{slab} + E_{S}^{slab} - E_{Al/S}^{interface})/A \quad (5)$$

where E (Al_2CO), E (SiC) and E (Al_2CO/SiC) represent the total energies of relaxed Al_2CO and SiC MLs and the Al_2CO/SiC heterostructure respectively. A represents the area of the interface. The optimized heterostructure and electronic properties are depicted in Fig. 3. The DOS analysis of the semiconductor heterostructure indicates that C and O atoms have a significant influence on the VB while Al and Si atoms make a significant contribution to the CB with strong interaction between interfaces due to the p_z orbital. The major states that contribute to the VBM were due to O-2p_z and C-2p_z, while Al-3p_z and Si-3p_z states mostly contribute to the CBM.[63] The electronic structure analysis of the heterostructure is crucial due to the presence of a C atom in both individual slabs. The C in Al_2CO forms a polar covalent bond due to its electronegative nature while the electropositive nature of Al implies that it carries a positive charge. When both C atoms combine to form a heterostructure they experience a different chemical environment. The Al_2CO higher chemical activity is due to its higher charge density and weaker bonding environment, while SiC's strong bonding within the lattice makes it less reactive resulting in electrons from Al_2CO flowing towards SiC. The C atom orbitals of Al_2CO and SiC can overlap, causing new energy states that alter the electronic structure of the heterostructure. The interface exhibits orbital overlap between Al-3p_z and Si-3p_z states, O-2p_z and C-2p_z states allowing orbital hybridization and facilitating the charge transfer across the heterostructure. The Hirshfeld charge analysis exhibits that Si atoms in the SiC ML transfer charge to O and C atoms. The Al atom exhibits different behavior when it comes to donating the charge to O and C during the formation of the heterostructure. These findings indicate that electrons are transported when both slabs come in contact forming the heterostructure (Fig. 1).

The Al_2CO/SiC heterostructure is dynamically and thermally stable.[63] The AIMD simulations were also performed at 300 K using an *NVT* ensemble for 10 000 steps with 0.5 fs time steps. Throughout the simulations, the equilibrium levels of temperature and energy were reached rapidly, and demonstrated that no structural deformation, bond breakage, or geometry relaxation can cover the original structure. These findings suggest that the Al_2CO/SiC heterostructure exhibits thermal stability at room temperature and higher.

3.2 Gas adsorption on SiC ML

All the gas molecules mentioned in the manuscript were considered in the investigation and were optimized in the gas phase prior to adsorption studies by using the GGA-PBE functional and computational details were clearly mentioned in the methodology section. The geometric structures of the gas molecules H_2O, NH_3, SO_2, NO, O_2 and H_2 were fully optimized as shown in Fig. 2, with bond lengths of 0.98, 1.00, 1.58, 1.15, 1.23, and 0.76 Å, respectively. Table 1 displays the bond lengths of gas molecules before and after optimizations.

We analyzed the interactions of six different gas molecules with SiC ML. First, we identified the stable adsorption site for molecular gases on SiC ML by considering four potential sites, such as silicon (Si), carbon (C), bridge (B), and hollow (H). The top and side views of optimized geometric structures for adsorbed molecules on SiC ML are represented in Fig. 3. The physisorption and chemisorption of gas molecules adsorbed on the surface were estimated by analyzing adsorption energies, charge transfer and the shortest bond distance between the molecule and ML. Physical adsorption occurs when the energy is less than 0.084 eV per molecule and chemical adsorption occurs when the energy is greater than 0.166 eV per molecule.[64,65]

First, we investigated H_2O adsorption on all possible sites and found that the Si site is the most preferable and stable with an E_{ads} of 0.90 eV as represented in Fig. 3. The H_2O molecule is positioned 3 Å above the SiC ML for optimization. The molecule interacts with SiC ML and forms a bond between the O atom in H_2O and the Si atom in SiC ML having bond distance of 2.01 Å after relaxation. The surface undergoes a slight distortion due to the adsorption of H_2O resulting in a change in the bond distance of Si–C to 1.81 Å while no changes occur in the H_2O molecule. The quantity of charge transferred from the surface to H_2O is $-0.15e$, indicating that the molecule makes a strong chemical bond with SiC ML related to chemical adsorption. Then, we investigated the NH_3 molecular adsorption. NH_3 is a trigonal pyramid shape composed of one nitrogen and three hydrogen atoms covalently bonded with nitrogen's valence electrons. The NH_3 molecule is positioned on all possible sites

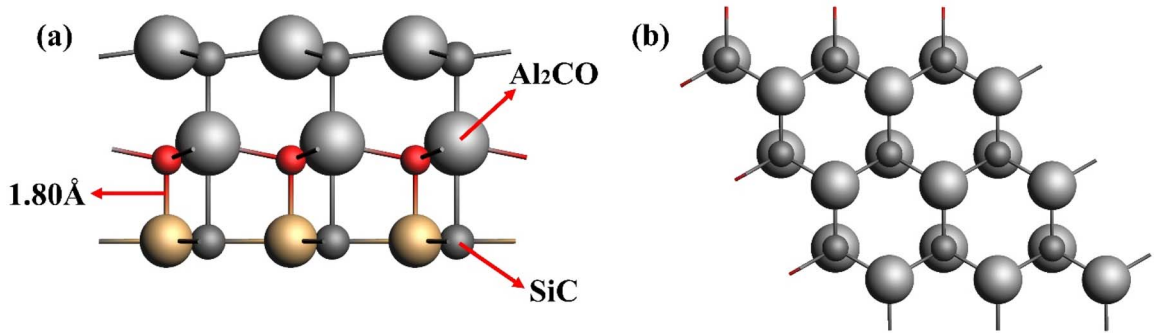

Fig. 1 Pictorial representation of the Al_2CO/SiC heterostructure: (a) side view and (b) top view.

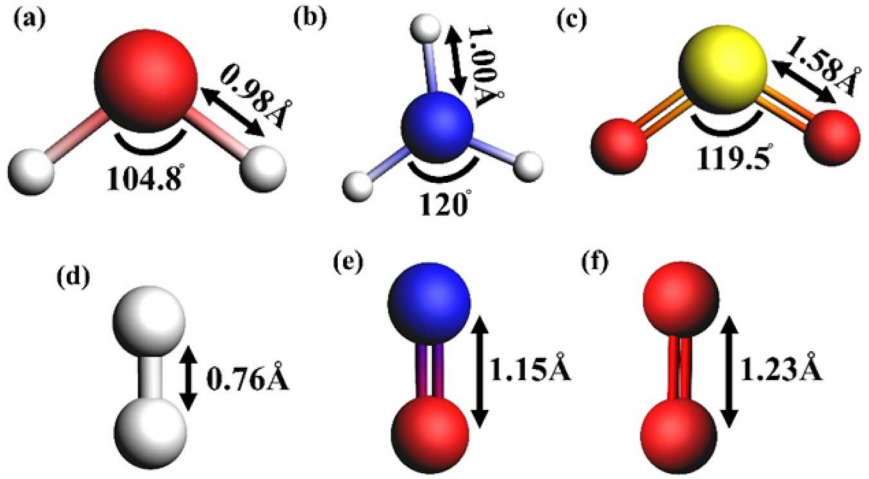

Fig. 2 The optimized structures of the gas molecules (a) H_2O, (b) NH_3, (c) SO_2, (d) H_2, (e) NO and (f) O_2.

Table 1 The bond lengths of molecules H_2O, NH_3, SO_2, NO, O_2, and H_2 before adsorption (l_0) and after adsorption (l) in Angstrom

Molecule	H_2O	NH_3	SO_2	NO	O_2	H_2
Length (l_o)	0.97	1.02	1.46	1.16	1.23	0.75
Length (l)	0.98	1.00	1.58	1.15	1.23	0.76

with 3 Å distance and the most stable geometries. The nitrogen atom in the NH_3 molecule forms a bond with the Si atom in SiC ML with a bond distance of 1.98 Å. The E_{ads} for this configuration is 1.17 eV and the amount of charge transferred from the molecule to ML is $-0.14e$. After optimization a slight structural deformation appears with a bond distance of 1.81 Å. The E_{ads}

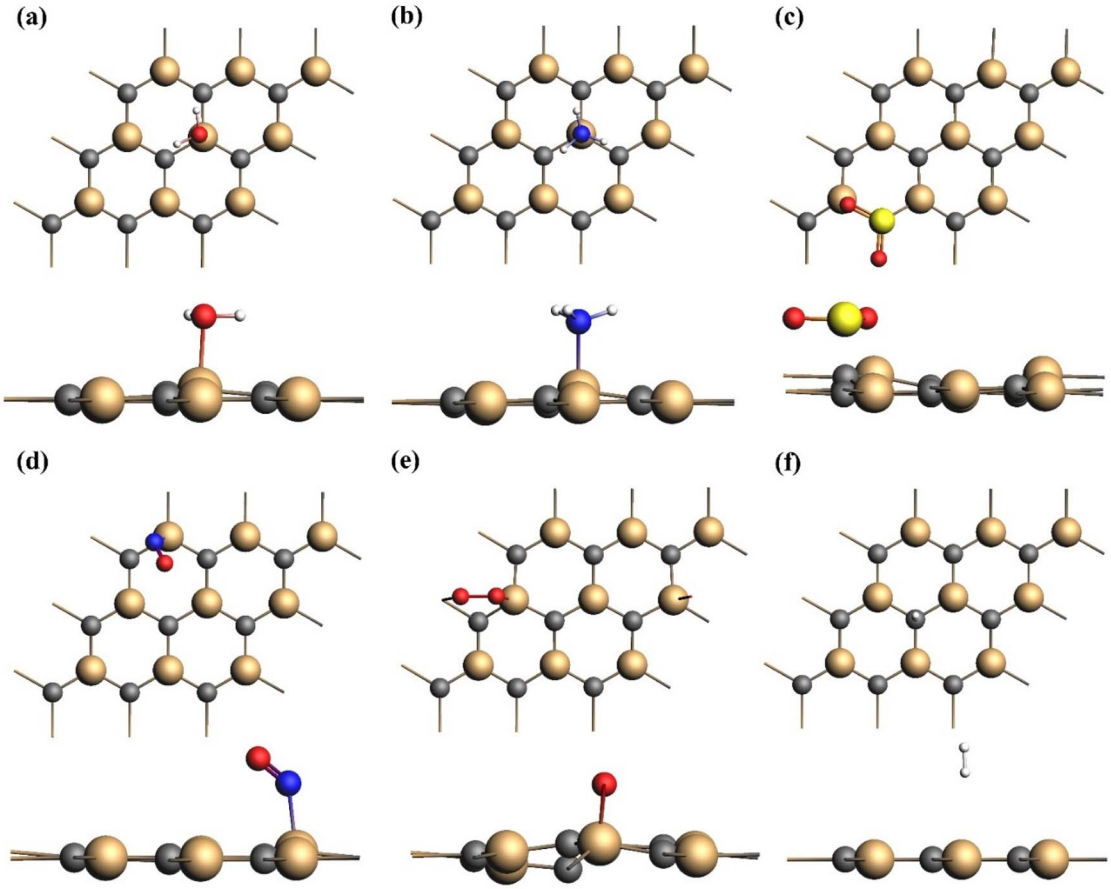

Fig. 3 Top and side views of the most energetically favorable optimized structures of SiC ML with gas adsorption: (a) H_2O, (b) NH_3, (c) SO_2, (d) NO, (e) O_2 and (f) H_2.

and charge transfer indicate that the NH_3 molecule is chemisorbed on SiC ML.

SO_2, NO, O_2 and H_2 molecules adsorbed on the SiC ML with the shortest distance between them being 1.80, 2.01, 1.01 and 2.72 Å respectively. The structural distortion occurred after SO_2 adsorption with an E_{ads} of 1.70 eV. The bond distances of Si–C, Si–Si and C–C were compressed to 1.79, 3.12, and 3.12 Å respectively. The charge analysis revealed that the S atom in the SO_2 molecule forms a chemical bond with the C atom in the SiC ML and Si atoms transfer 0.39e charge to the O (−0.199e) and C (−0.318e) atoms. The structural properties suggest that SO_2 is strongly adsorbed with a structural distortion and bond length compression, indicating chemical adsorption. The E_{ads} for NO, O_2, and H_2 are 0.80, 3.04, and 0.09 eV respectively. The slight structural distortion occurs after O_2 adsorption while no distortion appears after NO and H_2 adsorption. The NO adsorption forms a chemical bond with N–Si and behaves as a donor by transferring 0.342e and 0.036e charge to C (−0.338e) and O (−0.341e). Slight structural distortion occurred and the bond lengths of C–Si, Si–Si and C–C changed to 1.83, 3.05 and 3.14 Å after O_2 adsorption. The charge transfer process indicates that Si (0.348e) transfers the charge to C (−0.336e) and O (−0.107e). For H_2 adsorption, charge analysis indicates that the total charge on the molecule is −0.03e. The negative charge transfer value demonstrates that charge is transferred from ML to H_2. The minor charge transfer, low E_{ads} and large distance indicate minimal interaction between the H_2 molecule and the SiC ML. Hence, the adsorption in this case is physisorption. All gas molecules were strongly adsorbed on the SiC ML indicating chemisorption except for H_2. The adsorption of O_2 on the SiC ML exhibited high sensitivity due to strong interactions of gas molecules, large E_{ads}, charge transfer, and small vertical distance but the higher adsorption caused a challenge in desorbing the gas and also affected the sensor τ. The calculated values of E_{ads} the shortest distance between the gas molecule of the Al_2CO/SiC heterostructure,and charges for different adsorbed gases are given in Table 2.

3.3 Gas adsorption on the Al_2CO/SiC heterostructure

The potential of the Al_2CO/SiC heterostructure as a gas sensor is discussed in this section. The interactions between the molecules and changes in their structural and electronic properties are responsible for the selectivity of the material to be used as an efficient gas detector. To investigate the impact of gas adsorption on the Al_2CO/SiC heterostructure three adsorption sites, aluminum (A), carbon (B), and hollow (C) were considered to find the most stable adsorption configuration as depicted in Fig. S2. The most stable geometries of H_2O, NH_3, SO_2, NO, O_2, and H_2 gas molecules were found on the Al_2CO/SiC surface, as shown in Fig. 4. The graph indicates that H_2O prefers to be adsorbed on the C-site (hollow) where the formation energy is minimal. The H_2O molecule is placed in a perpendicular orientation above the surface. The B-site (carbon) is the preferred location for O_2, H_2, and SO_2 molecules with O_2 and SO_2 molecules parallel to the structure and H_2 perpendicular. The NH_3 molecule is positioned parallel to the surface while N points toward the surface and only this molecule finds the suitable A-site (Al). Fig. 6 depicts the most stable top and side views of the Al_2CO/SiC adsorption structures with molecules. The slight distortion of the heterostructure after adsorbing gas molecules depends on the gas molecule binding strength with the structure.

After the adsorption of the H_2O molecule on the heterostructures, the O atom formed a bond with Al due to its higher electronegativity compared to Al allowing it to pull electrons towards itself. This refers to the electron transfer process between gas molecules and the heterostructure. After adsorption, the length of the H_2O molecule changes from 0.97 Å to 0.98 Å indicating an elongation in bond length (O–H). The bond distance of O–Al is 2.11 Å which is larger than the sum of the covalent radii of connected atoms 2.09 Å. The calculated E_{ads} for H_2O on the heterostructure is 0.5 eV and the amount of electrons transferred from Al to O is 0.312 to −0.173e. The values obtained for E_{ads}, bond length and significant electron transfer indicate weak chemisorption. NH_3 was found to be adsorbed on the Al_2CO/SiC surface through an N–Al chemical bond with a bond distance of 2.11 Å which is smaller than the sum of the covalent radii of connected atoms is 2.13 Å. The N–Al bonding is due to the electronegativity difference that allows N to form

Table 2 The calculated values showing the type of adsorption, most favorable adsorption site, calculated values of adsorption energy (E_{ads}), the shortest distance between the gas molecule and the Al_2CO/SiC heterostructure (d), and charge analysis (Q)

Molecules	Position	E_{ads} (eV)	d (Å)	Q (e)
H_2O (chemisorption)	Si	0.90	2.01	−0.15
NH_3 (chemisorption)	Si	1.17	1.98	−0.14
SO_2 (chemisorption)	C	1.70	1.81	−0.19
NO (chemisorption)	Si	0.80	2.01	−0.02
O_2 (chemisorption)	Si	3.04	1.01	−0.11
H_2 (physisorption)	C	0.09	2.72	−0.02

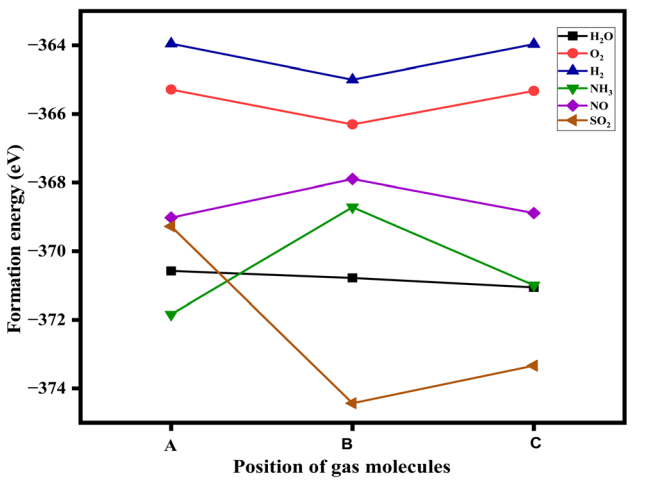

Fig. 4 Formation energies of all adsorbed molecules on the Al_2CO/SiC heterostructure, depending on different adsorption sites A, B, and C.

a coordinate covalent bond with Al and the electron transfer is −0.146*e* indicating that the charge is transferred from the Al_2CO/SiC surface to the NH_3 molecule. After adsorption, the length of the NH_3 molecule remains the same, which indicates no elongation in bond length (N–H). The calculated E_{ads} for this configuration is 0.68 eV, indicating strong chemical adsorption. The E_{ads} and adsorption distance for all adsorbed molecules on the Al_2CO/SiC heterostructure are represented in Fig. 5. The physisorption process involves a large adsorption distance and low E_{ads}, while the chemisorption process involves greater E_{ads} and a low adsorption distance.

On the Al_2CO/SiC heterostructure, SO_2 has an E_{ads} of 1.03 eV, with the B site being the preferred location for adsorption. SO_2 tends to form a bond with Al with an adsorption distance of 1.92 Å, smaller than the sum of covalent radii of connected atoms 2.09 Å and there was no obvious structural distortion. The distance of the SO_2 molecule changed from 1.46 Å to 1.57 Å indicating elongation. The charge analysis indicates that S, Si, and Al atoms act as donors and can transfer charge to C and O which behave as acceptors. The transfer of charge from the heterostructure to the gas molecule is 0.34*e*. The larger E_{ads} and smaller bond lengths of connected atoms indicate strong chemisorption. The most favorable configurations for all adsorbed gas molecules are represented in Fig. 6.

The E_{ads} for NO, O_2 and H_2 gas molecules were calculated to be 0.92, 2.14 and 0.03 eV with the adsorption distances of 2.05, 1.99 and 3.36 Å respectively. The NO molecule formed an N–Al bond with the Al_2CO/SiC heterostructure with no structural distortion. The distance of the NO molecule increased from 1.16 to 1.19 Å after adsorption and the amount of electron transfer from the surface to the gas molecule was 0.390*e*. These findings indicate that the NO molecule was chemisorbed on the Al_2CO/SiC heterostructure. In the case of O_2 adsorption, the O atom tends to form a bond with Al and the length of the O_2 molecule increases from 1.23 to 1.51 Å. The structural distortion of Al–O and Al–Al after O_2 adsorption showed slight variations being 2.06 and 3.61 Å respectively. In this case, the chemisorption behavior is strong due to significant charge transfer between O (−0.246*e*) and Al (0.349*e*). The results indicate that weak physisorption occurs in the case of H_2 adsorption due to the absence of charge transfer from the heterostructure to the gas molecule and the greater bond length of the bonded atom.

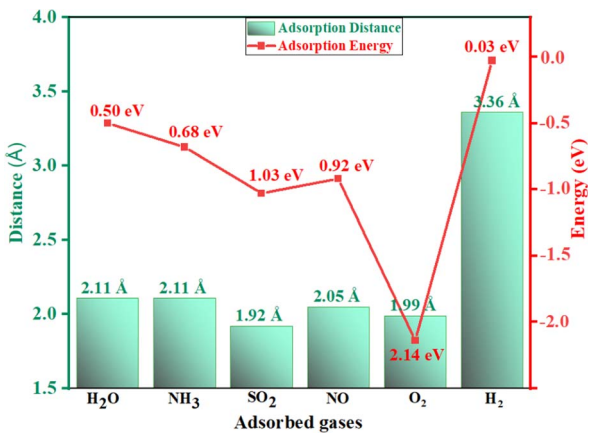

Fig. 5 The adsorption distance (Å) and E_{ads} (eV) of the Al_2CO/SiC heterostructure for various gas molecules.

The WF of the Al_2CO/SiC heterostructure was calculated after the adsorption of various gas molecules because it is crucial to accurately detect different gases; the results are shown in Fig. 7. The energy needed to transfer an electron from the system to infinity is known as WF and its variation directly impacts conductivity.[66,67] The WF can be calculated using eqn (6).[68]

$$\varphi = E_{vac} - E_F \quad (6)$$

where φ, E_{vac} and E_F denote the WF electrostatic potential at infinity and Fermi energy respectively. The WF of Al_2CO/SiC was 3.89 eV and no significant changes were observed after the adsorption of H_2O and H_2. On the other hand, the WF increased after the adsorption of SO_2, O_2, and NO but decreased after the adsorption of NH_3. The significant increases in WF after SO_2 and O_2 adsorption indicate a transition from a semiconductor to metallic nature while after NO adsorption, it increased to 0.12 eV. Therefore, we can conclude that Al_2CO/SiC is a promising gas sensor for detecting NO and NH_3 gas molecules and these results are consistent with E_{ads}. The sensor's sensitivity was calculated using eqn (4): for H_2O, it is 13.9%, NH_3 is 26.2%, SO_2 is 12.9%, H_2 is 15.9%, O_2 is 18.8% and NO is 3.1%. NH_3 has the highest sensitivity (26.2%), followed by O_2 (18.8%) and H_2 (15.9%) according to the results. On the other hand, NO has the lowest sensitivity (3.1%), indicating a poor heterostructure-interaction. This pattern demonstrates the outstanding capabilities of Al_2CO/SiC as a selective sensor particularly for NH_3 detection.

A comprehensive investigation was conducted for the charge analysis through the charge transfer integral of the host structure and the gas molecule H_2. It has been determined that CTI calculations are significant in analyzing the materials utilized in photochemistry and molecular electronics. The electron's ability to migrate between different orbitals and recombine from fragment 1 to fragment 2 and *vice versa* was measured. The electronic coupling V for hole transport and electron transfer was determined by DFTB to be 0.01 and 0.19 eV, respectively. For an electron that moved from fragment 1 to fragment 2, then recombines to return to its empty state, 0.02 eV is the calculated value of recombination between fragments 1 and 2, while 0.01 eV is the calculated value of recombination between fragments 2 and 1. The charge transfer integral reveals the charge analysis of the host structure and the gas molecule O_2. The electronic coupling V for hole transport and electron transfer is 0.14 and 0.08 eV, respectively. For an electron that moved from fragment 1 to fragment 2, then recombines to return to its empty state, 0.10 eV is the calculated value of recombination between fragments 1 and 2, while 0.06 eV is the calculated value of recombination between fragments 2 and 1.

The charge transfer integral reveals the charge analysis of the host structure and the gas molecule NH_3. The electronic coupling V for hole transport and electron transfer is 0.22 and 0.06 eV, respectively. For an electron that has been moved from fragment 1 to fragment 2, then recombines to return to its

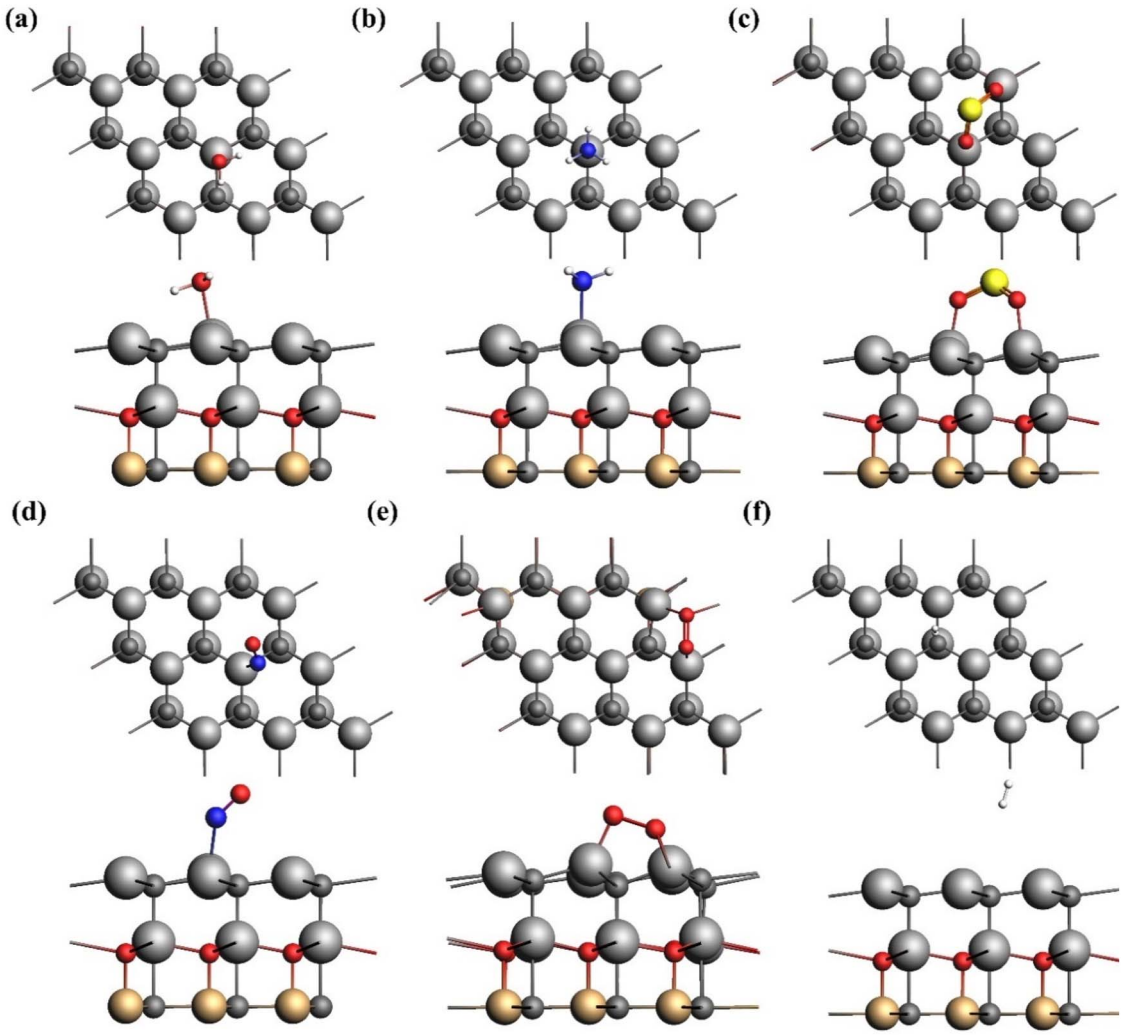

Fig. 6 The most favorable configurations for (a) H_2O, (b) NH_3, (c) SO_2, (d) NO, (e) O_2, and (f) H_2 adsorbed on the Al_2CO/SiC heterostructure.

empty state, 0.05 eV is the calculated value of recombination between fragments 1 and 2, while 0.01 eV is the calculated value of recombination between fragments 2 and 1. The charge transfer integral reveals the charge analysis of the host structure and the gas molecule H_2O. The electronic coupling V for hole transport and electron transfer is 0.18 and 0.03 eV, respectively. For an electron that has been moved from fragment 1 to fragment 2, then recombines to return to its empty state, 0.20 eV is the calculated value of recombination between fragments 1 and 2, while 0.03 eV is the calculated value of recombination between fragments 2 and 1. The summary of charge analysis, including the electronic coupling of electrons, holes, recombination rates from fragment 1 to 2 and 2 to 1, is given in Table 3.

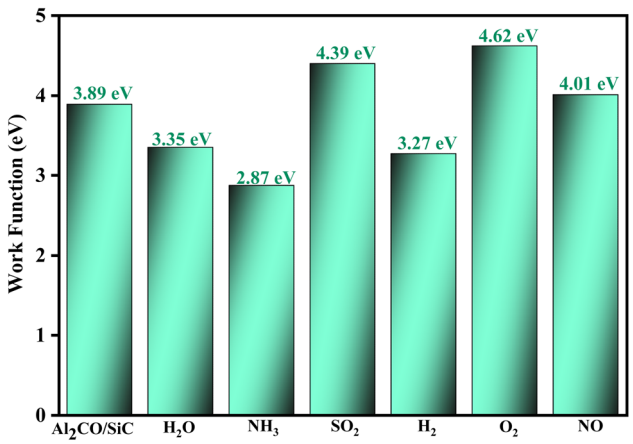

Fig. 7 WF of the Al_2CO/SiC heterostructure after the adsorption of various gas molecules.

3.4 The influence of the Al_2CO/SiC heterostructure on electronic properties after molecular adsorption

The study of the electronic structure is crucial for understanding the fundamental principles of gas sensing behavior and stronger adsorption. In this section, we will discuss the possible changes in the band structure and DOS of the Al_2CO/SiC heterostructure after gas molecule adsorption. There are two significant characteristics of the investigated cases. First, our findings demonstrate that the heterostructure exhibits

similar characteristics and retains its semiconductor properties. Secondly, the electronic properties after adsorption can change into metallic characteristics. The calculated band structures of the most favorable configurations are presented in Fig. 8. The band gap of the Al_2CO/SiC heterostructure significantly changed after adsorption, indicating that the adsorption of H_2O does not produce any impurity states with a slight variation from 1.38 to 1.30 eV. The band gap of the Al_2CO/SiC surface decreased to 1.18, 0.25 and 1.36 eV after the adsorption of NH_3, NO, and H_2 respectively. The Al_2CO/SiC heterostructure demonstrated minimal changes in the VB and CB after the adsorption of H_2O, NH_3, and H_2 retaining the direct band gap and semiconductor nature without spin up and down characteristics; therefore, the adsorptions did not introduce any magnetic properties. After NO adsorption, the impurity state appeared near the Fermi level, reducing the band gap but energy levels do not cross the Fermi level. Therefore, NO adsorption exhibits semiconductor properties with a 0.25 eV band gap and splits the spin degeneracy of the Al_2CO/SiC heterostructure into spin-up and down properties. The presence of the spin-down impurity states close to the Fermi level in the CB enhances the gas sensor's conductivity, indicating that NO adsorption has a magnetic nature. The impurity states promote the trapping action, which prevents electrons from combining with holes effectively. Initially, an electron moves in the CB instead of combining in the recombination center. Even trapped electrons increase the conductivity and relaxation time required to transition from the non-equilibrium to the equilibrium state, but do not take part in conduction directly.[69] Therefore, the Al_2CO/SiC heterostructure is a promising heterostructure for NO gas detection owing to its fascinating properties and efficient charge transport. Furthermore, after the SO_2 and O_2 adsorption the semiconductor nature of Al_2CO/SiC changes to metallic, reducing the band gap from 1.38 to 0 eV. The energy states in the VB overlap the Fermi level after SO_2 adsorption, and the Fermi level is close to the VB. The presence of spin-up and down states after O_2 adsorption indicates the magnetic properties and the Fermi level is close to the VB with spin-down states overlapping. The adsorption of SO_2 and O_2 on Al_2CO/SiC exhibits the same metallic properties, while O_2 shows magnetic characteristics.

Fig. S3 represents the DOS of the Al_2CO/SiC heterostructure after gas molecule adsorption and significant peaks transition from high to low energy positions. The DOS analysis exhibits electrical characteristics of Al_2CO/SiC can be changed in three different ways after molecular adsorption. First, the H_2O, NH_3, and H_2 adsorption do not significantly impact the VB and CB near the Fermi level, with a slight overlapping of orbitals below the Fermi level. The DOS spectra do not produce any additional states, but the band gap is reduced. It does not cause peak shifting and as a result no changes were observed. Second, after the adsorption of SO_2, a new peak was observed near the Fermi level which shifted towards the VB. It exhibits strong overlapping of orbitals and peaks shifting towards the left due to hybridization between the O 2p and S 3p orbitals in SO_2. The additional peak indicates the change in the behavior of the gas sensor from semiconductor to metallic. Third, the O_2 and NO adsorption show magnetic properties, and spin-polarized DOS are plotted in Fig. S3. After NO adsorption, new peaks appear close to the Fermi level in the CB reducing the band gap by 0.25 eV and the band shifted towards the left near the VB. The additional peaks are responsible for hybridizing the 2p orbitals of O and N. In the case of O_2, the spin-up and down states represent the bands that cross the Fermi level and induce unoccupied states in the CB. The Fermi level shifted towards the left near the VB indicating the transition from semiconducting to conducting properties. These findings illustrate the potential application of the Al_2CO/SiC heterostructure in gas sensors and confirm its selectivity for NH_3 and NO.

3.5 Gas sensing device evaluation

The selectivity and τ of the Al_2CO/SiC heterostructure were investigated in this section. The change in the Al_2CO/SiC band gap indicates the variation in the electrical conductivity which is represented by the formula below.[70]

$$\sigma \propto \exp\left[\frac{-E_g}{2KT}\right] \quad (7)$$

where σ represents electrical conductivity, E_g represents band gap, K represents Boltzmann constant (8.62×10^{-5} eV K^{-1}), and T indicates the thermodynamic temperature.[71] The correlation between band gap and conductivity is evident. The change in the band gap can be used to determine the conductivity changes after and before adsorption. Therefore, sensitivity can be determined using the change in conductivity (σ).[72,73] Electronic simulations revealed that every adsorbed surface had significantly smaller band gap energies than the isolated heterostructure. These findings suggest that adsorption has major impacts on the electronic properties of the Al_2CO/SiC heterostructure. The conductivity of the pure heterostructure at room

Table 3 The summary of charge analysis

No.	Gas molecule	Electronic coupling for electrons eV	Electronic coupling for holes eV	Recombination rate from 1 to 2 fragment	Recombination rate from 2 to 1 fragment
1	H_2	0.01	0.19	0.01	0.02
2	O_2	0.08	0.14	0.10	0.06
3	NO	0.01	0.05	0.28	0.09
4	SO_2	0.11	0.09	0.13	0.08
5	NH_3	0.06	0.22	0.05	0.01
6	H_2O	0.03	0.18	0.20	0.03

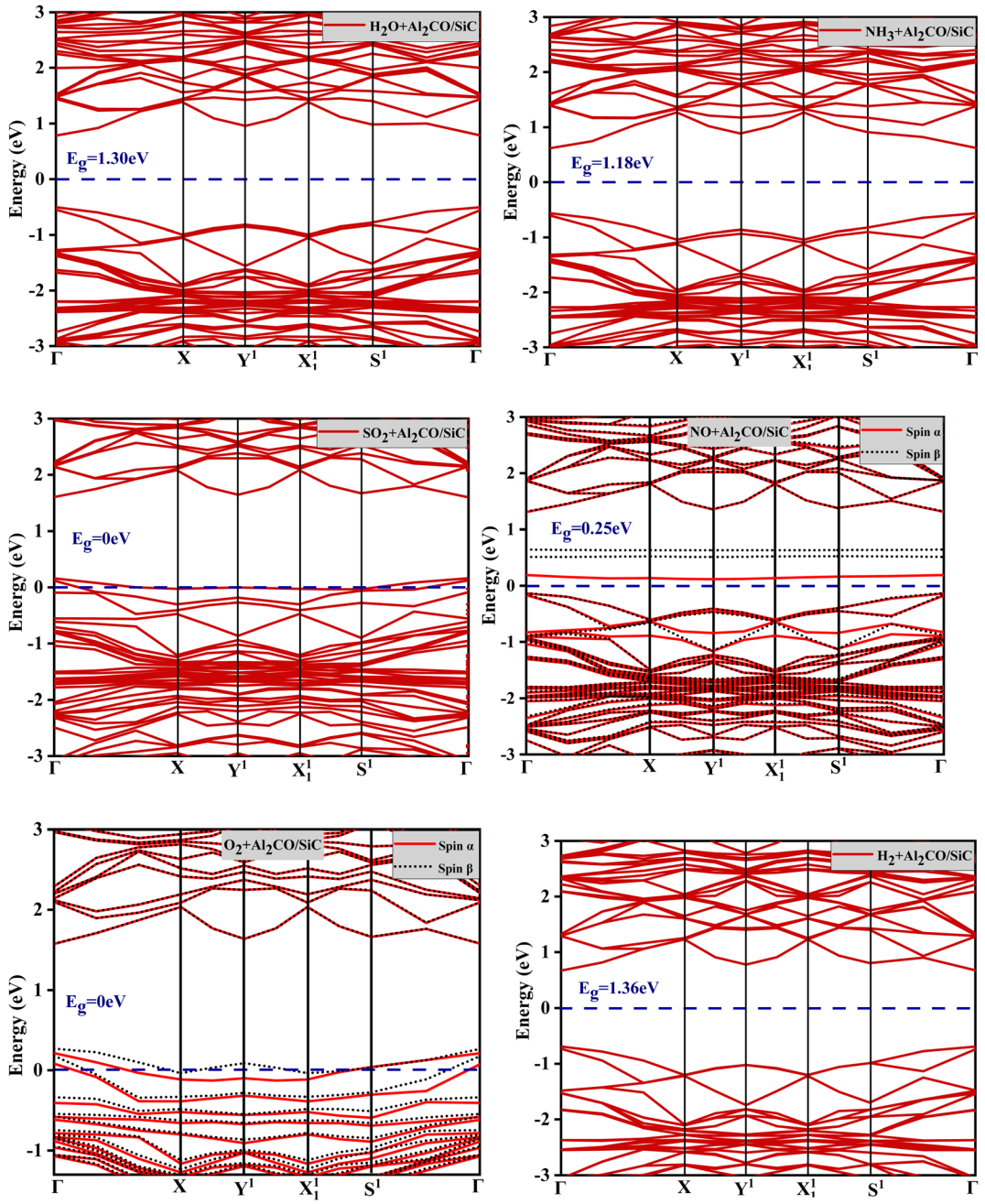

Fig. 8 The calculated band structures of the Al_2CO/SiC heterostructure after the adsorption of different gas molecules H_2O, NH_3, SO_2, NO, O_2, and H_2.

temperature (300 K) was found to be 2.58×10^{-12}. Table 4 presents the σ values of H_2O, NH_3, SO_2, NO, O_2, and H_2 gas molecules after adsorption.

The band gap of the Al_2CO/SiC heterostructure changed from 1.38 to 1.3 eV after the adsorption of H_2O molecules causing a minimal change in the conductivity. Similarly, after the H_2 adsorption, the band gap was reduced by 1.5% (1.38 to 1.36 eV) indicating slight changes in electronic properties. The nature of Al_2CO/SiC shifted from semiconductor to conductor after the adsorption of SO_2 and O_2 as the band gap decreased to 0 eV in these cases. After NO adsorption, the band gap was reduced to 0.25 eV, which is most suitable for gas sensing properties. Therefore, after H_2O, NH_3, SO_2, NO, O_2 and H_2 adsorption the band gaps changed to (0.08, 0.2, 1.38, 1.13, 1.38, and 0.02 eV) respectively. As a result, conductivities of the adsorbed gases were slightly altered except for SO_2 and O_2 due to their metallic character and significant changes were observed after NO adsorption. Chemisorption occurs in gases like H_2O, NH_3, SO_2, NO, and O_2 due to their larger E_{ads} and shorter distances while physisorption occurs in H_2. Therefore, the Al_2CO/SiC heterostructure demonstrates significant efficiency for detecting and sensing the H_2O, NH_3, SO_2, NO, and O_2 molecules.

The adsorption energy was also calculated using different XC functionals shown in Fig. 9. The trend of adsorption remains the same but the value of adsorption energy influences when GGA-PBE is used along with Grimes correction D3. Therefore, GGA-PBE-D3 is better than GGA-PBE because it includes van der Waals interactions and increases the accuracy.

The τ of a gas-detecting material is a crucial parameter for evaluating the effectiveness of a gas-sensing device. τ represents the sensor's reactivation duration and time taken for desorption from the surface. A tight binding between a gas molecule and the heterostructure renders it difficult to desorb from the surface; therefore, the sensor needs a lengthy recovery period. A shorter period of τ can be beneficial for gas sensor reversibility. Experimentally, τ is determined by heating the sensor at an elevated temperature, while it is computed theoretically *via* transition state theory using the van't Hoff–Arrhenius equation as follows:[74]

$$\tau = \nu^{-1} \exp\left[\frac{-E_{ads}}{k_B T}\right] \quad (8)$$

where ν represents the attempted frequency, and according to transition state theory, ν has a magnitude of 10^{13} s^{-1}.[75] k_B indicates the Boltzmann constant (8.62×10^{-5} eV K^{-1}). The temperature and adsorption energy are represented by T and E_{ads} respectively.[76] τ depends on E_{ads} and a gas exhibiting strong adsorption with the heterostructure takes longer to desorb. The τ for all adsorbed gas molecules on the Al_2CO/SiC heterostructure at 300 K are presented in Table 4. The Al_2CO/SiC heterostructure exhibits exceptionally higher E_{ads} for SO_2 and O_2 causing a significantly larger recovery period of 2.17×10^5 and 1.04×10^{24} s. As a result, direct use of the heterostructure as a gas sensor is hindered, and its reuse is limited for SO_2 and O_2. However, the Al_2CO/SiC shows moderate E_{ads} for NO and NH_3 leading to a rapid recovery period of 1.84×10^2 and 0.27 s, respectively. The shortest recovery duration exhibits immediate desorption for H_2O and H_2, specifically 2.60×10^{-4} and 3.19×10^{-12} s. The Al_2CO/SiC demonstrates exceptional selectivity and sensitivity for NO and NH_3 due to fast recovery and low conductivity changes making it a highly promising and reusable sensor. The H_2O and H_2 have weaker adsorption, rapid τ, and modest conductivity changes, making them useful for humidity sensors. On the other hand, the capture of SO_2 and O_2 was observed to be ineffective due to larger τ and conductivity, and might be used as a disposal alternative. Therefore, the order of strength of τ is $O_2 > SO_2 > NO > NH_3 > H_2O > H_2$. Future studies will explore the sensing performance of the Al_2CO/SiC heterostructure, focusing on the interactions of various gases like H_2S, to investigate potential applications. Our result indicates that SO_2 chemically adsorbs onto the material. However, sulfur toxicity can pose a threat to the substrate material, potentially affecting its long-term stability and functionality. Therefore, we plan to conduct further research to analyze the long-term effects of SO_2 adsorption on the substrate, focusing on its durability and structural stability during prolonged exposure to sulfur-containing gases. It is very crucial to analyze the adsorption behavior in the presence of multiple gases and evaluate the effect of humidity (water molecules). This would provide deeper insights into the practical application of our material. The future research will also explore the adsorption performance, selectivity, and sensitivity of the complex and practical applications of our material in real-world conditions by studying the effects of adsorption at different gas concentrations.

Table 4 The calculated values of σ and τ

Gas molecules	σ (S m^{-1})	τ (s)
H_2O	1×10^{-11}	2.60×10^{-4}
NH_3	1.2×10^{-10}	0.27
SO_2	1	2.17×10^5
NO	7.9×10^{-3}	1.84×10^2
O_2	1	1.04×10^{24}
H_2	3.8×10^{-12}	3.19×10^{-12}

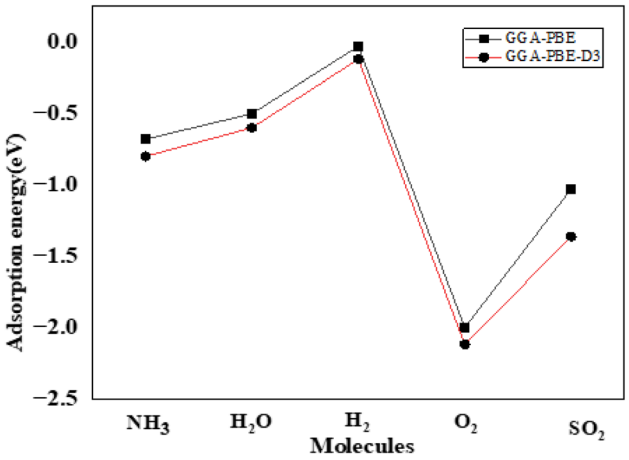

Fig. 9 The adsorption energies for H_2O, O_2, SO_2, NH_3, NO and H_2 molecules.

4. Summary

This work involves the adsorption and sensing behavior of different gas molecules (H_2O, NH_3, SO_2, NO, O_2, and H_2) on the SiC ML and the Al_2CO/SiC heterostructure. Structural, electronic and dynamical calculations were performed to explore the charge analysis, E_{ads}, sensitivity and τ at various sites after adsorption of the gas molecules. At first, we calculated the sensing behavior of SiC ML and all geometry optimizations were performed by using the GGA-PBE-D3 exchange–correlation functional. The findings demonstrate that for SiC ML the gas molecules H_2O, NH_3, SO_2, NO, and O_2 were chemisorbed due to greater E_{ads} and low adsorption distance. However, H_2 was physiosorbed due to lower E_{ads} and greater separation distance. Previous findings indicate that the SiC ML was considered a promising gas sensor for NH_3 detection, and has limited gas adsorption capabilities and selectivity owing to its higher band gap and minimal charge transfer ability. The Al_2CO/SiC heterostructure was designed with a low lattice mismatch to improve gas-detecting properties. The calculated E_{ads}

demonstrated that all gas molecules were chemisorbed on the heterostructure except H_2. The Hirshfeld charge analysis indicates that NH_3, O_2, H_2O, and NO are charge acceptors, while SO_2 is a charge donor, but H_2 is almost undetectable due to its minimal charge transfer. The band structure of Al_2CO/SiC undergoes significant changes after the adsorption of SO_2 and O_2, transitioning from a semiconductor to a metallic nature. Their strong adsorption enhances the conductivity, but desorption is a challenge. The band gap was reduced by 1.5% (1.38 to 1.36 eV), indicating slight changes in electronic properties after H_2 adsorption. The variation in the work function (WF) indicates that NO and NH_3 molecules exhibit a significant effect, which points to the potential application of the heterostructure in NO and NH_3 gas sensing due to their fast τ, low conductivity changes, larger sensitivity, and consistent adsorption behavior. Hence, the Al_2CO/SiC heterostructure is a highly effective 2D gas sensor capable of detecting NO and NH_3 gases at ambient temperature.

Conflicts of interest

The authors declare that they have no known competing financial interests or personal relationships that could have appeared to influence the work reported in this paper.

Data availability

The code for Amsterdam Density Functional (ADF) can be found at **https://www.scm.com**. The version of the code employed for this study is 2022.105.

Supplementary information is available. See DOI: **https://doi.org/10.1039/d5ra05654c**.

References

1 K. Y. Ko, *et al.*, Improvement of gas-sensing performance of large-area tungsten disulfide nanosheets by surface functionalization, *ACS Nano*, 2016, **10**(10), 9287–9296.
2 V. Kishnani, *et al.*, Highly sensitive, ambient temperature CO sensor using tin oxide based composites, *Sens. Actuators, A*, 2021, **332**, 113111.
3 J. Ding, *et al.*, The design of heterojunctions based on boron-/phosphorus-doped graphene and ZnO monolayer to enhance adsorption properties for toxic gases, *J. Appl. Phys.*, 2022, **131**(2), 025108.
4 B. khadim, *et al.*, The first-principles study on electronic transport mechanism in palladium decorated graphene for inert gas sensing, *Opt. Quantum Electron.*, 2024, **56**(3), 392.
5 A. Majid, *et al.*, Modeling of inert gas sensors using first principles methods, *IEEE Sens. J.*, 2023, **23**(16), 18118–18124.
6 W. Chaikittisilp, K. Ariga and Y. Yamauchi, A new family of carbon materials: synthesis of MOF-derived nanoporous carbons and their promising applications, *J. Mater. Chem. A*, 2013, **1**(1), 14–19.
7 J. Mi, *et al.*, A Cationic Polymerization Strategy to Design Sulfonated Micro–Mesoporous Polymers as Efficient Adsorbents for Ammonia Capture and Separation, *Macromolecules*, 2021, **54**(14), 7010–7020.
8 A. Hermawan, *et al.*, Advanced strategies to improve performances of molybdenum-based gas sensors, *Nano–Micro Lett.*, 2021, **13**, 1–46.
9 W. Yang, T. Chen and G. Zhou, Unveiling the tunable electronic, optoelectronic, and strain-sensitive gas sensing properties of Janus ZrBrCl: Insights from DFT study, *Appl. Surf. Sci.*, 2025, **680**, 161283.
10 A. Majid, *et al.*, Uncovering the Potential of Two-Dimensional SrRuO3 as anode material in Li, Na, Mg, Ca, K, and Zn ion Batteries: First-Principles investigations of structural, electronic and electrochemical properties, *J. Energy Storage*, 2025, **105**, 114634.
11 Z. Awang, Gas sensors: A review, *Sens. Transducers*, 2014, **168**(4), 61–75.
12 Y. Jian, *et al.*, Gas sensors based on chemi-resistive hybrid functional nanomaterials, *Nano–Micro Lett.*, 2020, **12**, 1–43.
13 S. Impeng, *et al.*, A MnN4 moiety embedded graphene as a magnetic gas sensor for CO detection: A first principle study, *Appl. Surf. Sci.*, 2019, **473**, 820–827.
14 S. Basu and P. Bhattacharyya, Recent developments on graphene and graphene oxide based solid state gas sensors, *Sens. Actuators, B*, 2012, **173**, 1–21.
15 J. R. Stetter and J. Li, Amperometric gas sensors a review, *Chem. Rev.*, 2008, **108**(2), 352–366.
16 G. Jiang, *et al.*, Free-standing functionalized graphene oxide solid electrolytes in electrochemical gas sensors, *Adv. Funct. Mater.*, 2016, **26**(11), 1729–1736.
17 J. Hodgkinson and R. P. Tatam, Optical gas sensing: a review, *Meas. Sci. Technol.*, 2012, **24**(1), 012004.
18 C. Zhang, P. Chen and W. Hu, Organic field-effect transistor-based gas sensors, *Chem. Soc. Rev.*, 2015, **44**(8), 2087–2107.
19 A. Bag, *et al.*, Room-temperature-operated fast and reversible vertical-heterostructure-diode gas sensor composed of reduced graphene oxide and AlGaN/GaN, *Sens. Actuators, B*, 2019, **296**, 126684.
20 S. Kim, *et al.*, Thermochemical hydrogen sensor based on chalcogenide nanowire arrays, *Nanotechnology*, 2015, **26**(14), 145503.
21 S. Kim, *et al.*, Facial fabrication of an inorganic/organic thermoelectric nanocomposite based gas sensor for hydrogen detection with wide range and reliability, *Int. J. Hydrogen Energy*, 2019, **44**(21), 11266–11274.
22 E. Vereshchagina, *et al.*, Low power micro-calorimetric sensors for analysis of gaseous samples, *Sens. Actuators, B*, 2015, **206**, 772–787.
23 A. Harley-Trochimczyk, *et al.*, Low-power catalytic gas sensing using highly stable silicon carbide microheaters, *J. Micromech. Microeng.*, 2017, **27**(4), 045003.
24 Z. Meng, *et al.*, Electrically-transduced chemical sensors based on two-dimensional nanomaterials, *Chem. Rev.*, 2019, **119**(1), 478–598.
25 M. Barzegar and B. Tudu, Two-dimensional materials for gas sensors: from first discovery to future possibilities, *Surf. Innovations*, 2018, **6**(4–5), 205–230.

26 H. Zhang, M. Chhowalla and Z. Liu, 2D nanomaterials: graphene and transition metal dichalcogenides, *Chem. Soc. Rev.*, 2018, **47**(9), 3015–3017.
27 H. Batool, *et al.*, A DFT study of quantum electronic transport properties of InTeCl, *Mater. Sci. Semicond. Process.*, 2023, **168**, 107842.
28 A. C. Ferrari, *et al.*, Science and technology roadmap for graphene, related two-dimensional crystals, and hybrid systems, *Nanoscale*, 2015, **7**(11), 4598–4810.
29 A. Jabeen, *et al.*, Impacts of structural downscaling of inorganic molecular crystals-A DFT study of Sb2O3, *Mater. Sci. Semicond. Process.*, 2023, **166**, 107729.
30 A. Majid, *et al.*, Prospects of ruthenate-based electrodes in metal-ion batteries, *Sustain. Energy Fuels*, 2024, **8**(18), 4019–4038.
31 O. Leenaerts, B. Partoens and F. Peeters, Adsorption of H 2 O, NH 3, CO, NO 2, and NO on graphene: A first-principles study, *Phys. Rev. B: Condens. Matter Mater. Phys.*, 2008, **77**(12), 125416.
32 Z. Ao, *et al.*, Enhancement of CO detection in Al doped graphene, *Chem. Phys. Lett.*, 2008, **461**(4–6), 276–279.
33 C. Luo, *et al.*, Susceptible Detection of Organic Molecules Based on C3B/Graphene and C3N/Graphene van der Waals Heterojunction Gas Sensors, *ACS Sens.*, 2024, **9**(9), 4822–4832.
34 A. Majid, *et al.*, Unraveling the potential of Al2CO bilayer as anode material in magnesium ion battery and unsuitability for lithium ion battery, *J. Alloys Compd.*, 2024, **981**, 173697.
35 H. Batool, *et al.*, On the prospects of solid state hydrogen storage: First-principles investigations of two-Dimensional In2CO, *Int. J. Hydrogen Energy*, 2024, **95**, 510–519.
36 S. Z. Butler, *et al.*, Progress, challenges, and opportunities in two-dimensional materials beyond graphene, *ACS Nano*, 2013, **7**(4), 2898–2926.
37 A. Majid, *et al.*, On the prospects of using B4C3 as a potential electrode material for lithium-ion batteries, *Mater. Sci. Semicond. Process.*, 2024, **176**, 108320.
38 A. Yaghoubi, *et al.*, Is graphitic silicon carbide (silagraphene) stable?, *Chem. Mater.*, 2018, **30**(20), 7234–7244.
39 A. Sultan, S. Ahmad and F. Mohammad, A highly sensitive chlorine gas sensor and enhanced thermal DC electrical conductivity from polypyrrole/silicon carbide nanocomposites, *RSC Adv.*, 2016, **6**(87), 84200–84208.
40 J. Chen, *et al.*, High-temperature hydrogen sensor based on platinum nanoparticle-decorated SiC nanowire device, *Sens. Actuators, B*, 2014, **201**, 402–406.
41 Z. Shi, *et al.*, Predicting two-dimensional silicon carbide monolayers, *ACS Nano*, 2015, **9**(10), 9802–9809.
42 H. Dong, *et al.*, Theoretical investigations on novel SiC5 siligraphene as gas sensor for air pollutants, *Carbon*, 2017, **113**, 114–121.
43 G. Gao, S. H. Park and H. S. Kang, A first principles study of NO2 chemisorption on silicon carbide nanotubes, *Chem. Phys.*, 2009, **355**(1), 50–54.
44 Z. Zhao, *et al.*, Gas-sensing properties of the SiC monolayer and bilayer: a density functional theory study, *ACS Omega*, 2020, **5**(21), 12364–12373.
45 R. Wu, *et al.*, Silicon carbide nanotubes as potential gas sensors for CO and HCN detection, *J. Phys. Chem. C*, 2008, **112**(41), 15985–15988.
46 V. Babar, S. Sharma and U. Schwingenschlögl, New paradigm for gas sensing by two-dimensional materials, *J. Phys. Chem. C*, 2019, **123**(20), 13104–13109.
47 X. Dong, T. Chen and G. Zhou, Design high performance field-effect, strain/gas sensors of novel 2D penta-like Pd2P2SeX (X= O, S, Te) pin-junction nanodevices: A study of transport properties, *J. Alloys Compd.*, 2024, **977**, 173417.
48 A. Majid, *et al.*, Electrochemical Performance of P4Se3 as High-Capacity Anode Materials for Monovalent and Multivalent Ion Batteries, *Mater. Chem. Phys.*, 2024, 129515.
49 S. Khammuang, A. Udomkijmongkol, S. Thasitha and T. Hussain, Komsilp Kotmool First-principles study insights into Janus MoWC-based MXenes for enhanced H2S and NH3 sensing applications, *Appl. Surf. Sci.*, 2025, **699**, 163110.
50 S. Khammuang, K. Wongphen and T. Hussain, Komsilp Kotmool Enhanced NH 3 and NO sensing performance of Ti 3 C 2 O 2 MXene by biaxial strain: insights from first-principles calculations, *Phys. Chem. Chem. Phys.*, 2025, **27**(7), 3827–3833.
51 H. Vovusha, H. Bae, S. Lee, J. Park, R. Ali, K. Kotmool and T. Hussain, Hoonkyung Lee Density functional theory studies of MXene-based nanosensors for detecting volatile organic compounds in meat spoilage assessment, *ACS Appl. Nano Mater.*, 2023, **6**(19), 18592–18601.
52 M. Ueland, H. Bae, A. Udomkijmongkol, K. Kotmool, V. Gulati and T. Hussain, Single atom dispersed tungsten disulfide (WS2) based nanosensors for VOCs detection related to decomposed humans in disaster events, *FlatChem*, 2024, **45**, 100666.
53 P. Panigrahi, K. Kotmool, S. Khammuang, H. Bae, V. Gulati and T. Hussain, Smart Sensing Characteristics of Tungsten Diselenide (WSe2) Monolayers toward Depression-Related Volatile Organic Compounds, *ACS Appl. Nano Mater.*, 2025, **8**(11), 5685–5693.
54 L. Liao, *et al.*, High-speed graphene transistors with a self-aligned nanowire gate, *Nature*, 2010, **467**(7313), 305–308.
55 G. t. Te Velde, *et al.*, Chemistry with ADF, *J. Comput. Chem.*, 2001, **22**(9), 931–967.
56 L. Hedin, New method for calculating the one-particle Green's function with application to the electron-gas problem, *Phys. Rev.*, 1965, **139**(3A), A796.
57 J. Heyd, G. E. Scuseria and M. Ernzerhof, Hybrid functionals based on a screened Coulomb potential, *J. Chem. Phys.*, 2003, **118**(18), 8207–8215.
58 X. Ke, G. J. Kramer and O. M. Løvvik, The influence of electronic structure on hydrogen absorption in palladium alloys, *J. Phys.: Condens. Matter*, 2004, **16**(34), 6267.
59 A. Becke, Accurate local approximation to the exchange-correlation density functional: the MN12-L functional for electronic structure calculations in chemistry and physics, *Opt. Phys.*, 1988, **38**, 3098–3100.

60 S. Nosé, A unified formulation of the constant temperature molecular dynamics methods, *J. Chem. Phys.*, 1984, **81**(1), 511–519.
61 Y. Jin, *et al.*, Enhanced adsorption properties of ZnO/GaN heterojunction for CO and H2S under external electric field, *Comput. Theor. Chem.*, 2021, **1206**, 113495.
62 V. Ilyasov, *et al.*, Adsorption of atomic oxygen, electron structure and elastic moduli of TiC (0 0 1) surface during its laser reconstruction: Ab initio study, *Appl. Surf. Sci.*, 2015, **351**, 433–444.
63 A. Shehbaz, *et al.*, Probing the potential of Al 2 CO/SiC heterostructures for visible light-driven photocatalytic water splitting using first-principles strategies, *J. Mater. Chem. A*, 2024, **12**(21), 12657–12671.
64 M. S. Onyango, *et al.*, Adsorption equilibrium modeling and solution chemistry dependence of fluoride removal from water by trivalent-cation-exchanged zeolite F-9, *J. Colloid Interface Sci.*, 2004, **279**(2), 341–350.
65 S. Tahir and N. Rauf, Removal of a cationic dye from aqueous solutions by adsorption onto bentonite clay, *Chemosphere*, 2006, **63**(11), 1842–1848.
66 M. S. Islam, *et al.*, Augmenting the sensing aptitude of hydrogenated graphene by crafting with defects and dopants, *Sens. Actuators, B*, 2016, **228**, 317–321.
67 B. Wang, J. Nisar and R. Ahuja, Molecular simulation for gas adsorption at NiO (100) surface, *ACS Appl. Mater. Interfaces*, 2012, **4**(10), 5691–5697.
68 A. Kiejna and K. F. Wojciechowski, *Metal Surface Electron Physics*, Elsevier, 1996.
69 N. Mishra, *et al.*, Enhanced electronic and magnetic properties of N 2 O gas adsorbed Mn-doped MoSe 2 monolayer, *IEEE Trans. Electron Devices*, 2021, **69**(4), 1634–1641.
70 F. Opoku and P. P. Govender, Adsorption behaviour of Si anchored on g-C3N4/graphene van der Waals heterostructure for selective sensing of toxic gases: Insights from a first-principles study, *Appl. Surf. Sci.*, 2020, **525**, 146590.
71 M. Manoilo, B. Mischanchuk and É. Korol', Mechanism of the conduction of thin composite films of polyethylene and metals, *Theor. Exp. Chem.*, 1991, **27**(5), 545–547.
72 L. Kou, T. Frauenheim and C. Chen, Phosphorene as a superior gas sensor: selective adsorption and distinct I–V response, *J. Phys. Chem. Lett.*, 2014, **5**(15), 2675–2681.
73 J. Prasongkit, *et al.*, Highly sensitive and selective gas detection based on silicene, *J. Phys. Chem. C*, 2015, **119**(29), 16934–16940.
74 V. B. T. Phung, *et al.*, Graphene as a Sensor for Lung Cancer: Insights into Adsorption of VOCs Using vdW DFT, *ACS Omega*, 2024, **9**(2), 2302–2313.
75 A. Kokalj, Formation and structure of inhibitive molecular film of imidazole on iron surface, *Corros. Sci.*, 2013, **68**, 195–203.
76 K. Yamaguchi, *et al.*, A spin correction procedure for unrestricted Hartree-Fock and Møller-Plesset wavefunctions for singlet diradicals and polyradicals, *Chem. Phys. Lett.*, 1988, **149**(5–6), 537–542.